Full-fiber ellipsometry

The (im)possibility of eliminating line-of-sight

Bruno van Albada

March 15, 2013

Abstract

Ellipsometry is a non-contact, extremely accurate technique for characterising thin films, which over the past decades have become vital in a host of applications. However, ellipsometry suffers from a number of disadvantages, the most inconvenient of which are that it requires line-of-sight access to the sample, and demands careful calibration of any optical components. Succeeding in building an ellipsometer that does not require line-of-sight could severely reduce especially *in situ* measurement complexity, as well as allowing a single ellipsometer to be timeshared over multiple setups, forming a significant cost reduction. In this work, an ellipsometry setup that uses optical fibers in lieu of direct line-of-sight is investigated. We demonstrate that the output polarisation states from such a full-fiber ellipsometer form a well-defined band on the Poincaré sphere, which is preserved and can be seen as a generalised polarisation state. Changes to this generalised polarisation state can then be used to obtain the ellipsometric angles Ψ and Δ from a given sample. Provided the setup is well-characterised, the accuracy is comparable to that of conventional ellipsometry.

Contents

1 Introduction

Over the past decades, thin films – meaning layers of material with a thickness between one monolayer and approximately a micrometer – have become vital in a host of applications, such as solar cells [1], drug delivery [2, 3], (anti-)reflective coatings [4, 5] and the semiconductor industry [6, 7]. This increase in thin-film applications has (naturally) been accompanied by an enormous increase in interest for characterisation methods, and a huge number of methods are now available. However, nearly all of these techniques have one or more significant downsides. Microscopy techniques, such as scanning electron microscopy and transmission electron microscopy, while extremely useful for imaging samples at very high resolutions, reveal fairly little about sample composition and often require extensive sample preparation. Methods that excel at detecting sample composition, such as Rutherford backscattering spectrometry and Auger electron spectroscopy, have to be performed in vacuum and use high-energy beams that often damage the sample surface. Other methods, such as atomic force microscopy and X-ray photoelectron spectroscopy, come with their own distinct set of advantages and disadvantages. In general, it can be said that there seem to be no 'easy' methods for characterising a thin film.

Another method for characterising thin films is ellipsometry. It is a non-contact, non-destructive, yet extremely sensitive technique, and as such, seems very well suited for thin-film characterisation. Ellipsometry works by reflecting light with a known polarisation state off a sample – here, a thin film. This light will be partially reflected off the top film/air interface, as well as off the bottom substrate/film interface, creating a phase shift between the two reflected beams that is dependent on the sample's refractive index as well as its thickness. This phase shift causes interference between the two beams, which, in turn, causes a phase shift in the light returning from the sample. In addition, the polarisation state of the reflected light is heavily dependant on the Fresnell reflection coefficients, which are polarisation-dependant. Finally, scattering and absorption also modify the polarisation state of the reflected light.[1] Ellipsometry, then, is the process of accurately determining the refractive index, optical absorption, scattering and physical thickness of a thin film by analysing the changes in polarisation. Because polarisation can be measured with high precision and sensitivity, even very small polarisation changes, caused by layers much thinner than the wavelength of the light used, can be accurately quantified. This makes

[1] All this is explained in more detail in Section 2.

ellipsometry an ideal tool for surface analysis.

Since it is so crucial to accurately determine the polarisation state when performing ellipsometry, great care must be taken to ensure that it is only the sample which introduces an unpredictable polarisation change. Thus, in general, all optical elements introduced to the ellipsometry configuration must have a fixed effect on the polarisation state, which can be calibrated for in the measurement. Such elements might be glass plates, or beam splitters, but not wave guides. For this reason, *in situ* applications of ellipsometry have so far been limited by the accessibility of the sample, as line of sight is needed to perform accurate measurements. While setups involving chamber windows to provide line of sight access are certainly possible [8], these methods are generally more expensive and cumbersome than *ex situ* ellipsometry as all optical elements require careful calibration.. Furthermore, such an ellipsometer can only be used on one specific chamber at a time, meaning that if multiple chambers require *in situ* measurements simultaneously, separate ellipsometers have to be bought for every chamber, further increasing costs. Thus, so far ellipsometry has served as a useful and accurate technique, hampered by practical constraints. A 'moveable' *in situ* ellipsometer that does not require direct line of sight would mean a huge cost reduction, as a single, time-shared ellipsometer would be sufficient to service a whole lab, both for *in situ* and *ex situ* applications. Secondly, such a technique would help greatly in making ellipsometry more accessible for difficult and crowded measurement setups.

Several researchers have attempted to tackle this problem by introducing optical fibers to replace the otherwise free space optical path between the polarising and analysing module – *fiber* ellipsometry [9, 10]. By using optical fibers, light can be more easily introduced into sensitive environments and be transported over relatively long distances. However, fibers do come with a very significant disadvantage: ordinary fibers do not preserve polarisation. This can be (partially) solved by introducing an optical axis into the fiber, which breaks the rotational symmetry of an ordinary fiber. These fibers are called Polarisation-Maintaining (PM) Fibers. Unfortunately, PM fibers will only preserve two specific polarisation states with certainty, while the others undergo a time dependent change which is apparently random for each individual measurement [11]. An example of this can be seen in Fig. 1.1, which plots the horizontal component of light exiting a PM fiber over time for a constant input polarisation. This Stokes vector component varies in the range $\in [-1, 1]$, and while an overall trend can be seen, it is clear that the light exiting the fiber will not have a clearly predictable polarisation state. The mechanism behind this is explained in Section 2.4.

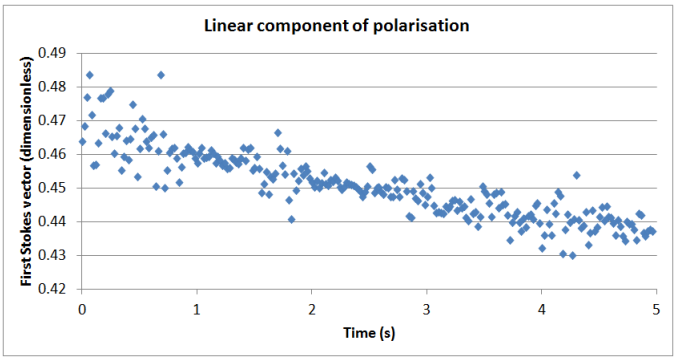

Figure 1.1: The horizontal component of the polarisation state (the first Stokes vector, $\in [-1, 1]$), of light exiting a PM fiber, plot against time. Note that while a trend can be identified, it is impossible to predict what polarisation state the light will have at any given time.

In summary: contrary to what the name suggests, polarisation-maintaining fibers do not preserve arbitrary polarisation states. Thus, when performing fiber ellipsometry, the polarisation state of light reflected off the sample (in principle, any arbitrary state) will not be preserved by the fiber that transports this light from the sample to the analysing module, except in very rare cases. As a result, fiber ellipsometry has not seen much use, limited by very complicated measurement setups [12] and/or an inability to perform quantitative measurements [9]. If this problem could be solved, this would be an enormous step towards the moveable, non-line-of-sight ellipsometer described above.

1.1 Previous work

When the polarisation states are measured in the Stokes vector basis, then, they naturally fall on a sphere, called the Poincaré sphere. If the output polarisation states from a PM fiber were truly random, then a single input polarisation state would result in an infinite number of output polarisation states that, when projected onto the the Poincaré sphere, would gradually fill the entire surface of the sphere. However, this is not the case. Previous work by this group has shown that instead, the output polarisation states fall on a single well-defined, one-dimensional orbit on the Poincaré sphere. This orbit is independent of all the environmental parameters that affect the individual polarization. The orientation of this orbit is the key to performing ellipsometry without knowing the precise polarisation state

of the incident light [13]. By treating this orbit as a generalised, higher dimensional polarisation state, the changes to the orientation of the orbit can be used in place of individual polarisation states to perform ellipsometry. This method was used to accurately measure the difference between a 0.3 and 0.8 nm layer of hydrogenated carbon using a "half-fiber" ellipsometer: i.e. an ellipsometer where a fiber is used for transporting the light to the sample, but after reflection, the light is propagates through free space to the polarimeter [13]. Thus, the consequences of using an optical fiber – more precisely, a polarisation-maintaining optical fiber – for transporting light to the sample are known, and can be compensated for. More on this method, and the theory behind it, can be found in Section 2. This section also includes the mathematics of a polarisation-maintaining fiber, which previous work has also studied in detail.

1.2 Goal and method

In this work, an attempt will be made to construct a 'full' fiber ellipsometer, which is to say an ellipsometer where the probing light is transported to and from the sample using optical fibers. The eventual goal for this project is to build a fully working fiber ellipsometer with accuracy comparable to that of conventional ellipsometry.

In this process, three important sub-goals can be identified:

1. Understanding fiber behaviour, both mathematically and experimentally, for single-fiber systems as well as for double-fiber ones.

2. To develop a solution that allows the ellipsometry parameters Ψ and Δ to be extracted from the data, using the insights gathered in step 1.

3. Testing this solution and accuracy and reliability of the fiber ellipsometer by comparing it to a conventional ellipsometer using well-defined samples

The remainder of this thesis provides a description of the theoretical work, modelling and experiments that we have performed to achieve these goals. In Section 2, we introduce the most important concepts of previous work done by this group, as well as the mathematical background of polarisation, ellipsometry, polarisation-maintaining fibers, and the half-fiber ellipsometer. In Section 3, we describe the physics and mathematical model used to understand and predict the behaviour of polarisation maintaining

fibers. Additionally, we give a mathematical model for extracting the ellipsometry parameters from a two-fiber system. In Section 4, experimental results of tests to our solution of the convolution problem are given. Finally, Section 5 highlights the most important conclusions from this work, as well as suggestions for future research. In the appendix, experimental results on the polarisation behaviour of a more stable photonic crystal fiber are described.

2 Fiber theory

2.1 Polarisation

In order to perform ellipsometry measurements, information about the polarisation state of the light, both incident and reflected from the sample, is needed. Why this is will be explained in section 2.2, below, but the focus will first be on explaining the principle of polarisation.
Light waves, unlike sound waves, do not, in general, oscillate in the same direction they travel in. Instead, they are transverse waves, oscillating perpendicular to the direction of energy transfer. The polarisation state of a wave is a way of describing how the spatial orientation of the fields that make up a wave varies in time. The electromagnetic field is made up of two mutually perpendicular fields, which oscillate in a plane that is perpendicular to the travel direction: the electric and the magnetic field. Since the magnetic field is always perpendicular and proportional to the electric field, it can be ignored and only the electric field needs to be considered. Assuming a simple, sinusoidal wave in Cartesian coordinates, the projection of the electric field amplitude into the x and y directions (with z indicating the direction of travel) can be described as follows:

$$E_x = a\cos(\theta) \tag{2.1}$$
$$E_y = b\cos(\theta + \phi) \tag{2.2}$$

Here, θ is given by $kz - \omega t$, with k the wave number and ω the angular frequency, with a and b the maximum amplitude for the the two projections, respectively, and ϕ the phase difference between the two waves. it is important to note that it is the relative values of a and b that are important; the polarisation does not change when ϕ and $\frac{a}{b}$ are both constant.

It can easily be seen from these equations that light can have an infinite number of polarisation states. Polarisation states can be broadly described by the shape traced by the sum of equations 2.1 and 2.2 in the $x - y$ plane; varying from light linearly polarised along the x or y axis (for example, when a or b is zero), to circularly polarised light when $a = b$ and $\phi = -\frac{\pi}{2}$. More generally, the polarisation state of the light is known as the *polarisation ellipse* [14].

In this thesis, the Stokes parameters will be used to characterise the polarisation ellipse, as this is convenient when doing ellipsometry (as will be seen below). Following the notation conventions outlined above, these four

parameters are defined as follows:

$$I = a^2 + b^2 \tag{2.3}$$

$$P_1 = a^2 - b^2 \tag{2.4}$$

$$P_2 = 2ab\cos(\phi) \tag{2.5}$$

$$P_3 = 2ab\sin(\phi) \tag{2.6}$$

These four parameters characterise three independent variables, since $I^2 = P_1^2+P_2^2+P_3^2$.[2] In terms of the polarisation ellipse intensity, I, of the light[3], P_1 describes the amount of light that is linearly polarised along two orthogonal axes, horizontal (+) or vertical (-) directions, for example. P_2 describes light that is linearly polarised at 45° to the orthogonal axes, and P_3, light that is circularly polarised. Stokes vectors are usually normalised, meaning that $I^2 = 1$ and $P_1, P_2, P_3 \in [-1, 1]$. Since $P_1^2 + P_2^2 + P_3^2 = 1$, the the total magnitude of the Stokes vector is constrained. This, combined with P_1, P_2 and P_3 ranging from -1 to 1, means these values can be portrayed as points on a sphere. This sphere is called the Poincaré sphere, each point on the sphere representing a specific polarisation state.[14]
Now, the remaining issue is to describe how optical components modify the polarisation state. We will define the initial polarisation state of the light as $\vec{S_0}$, the optical component as M and the resulting output light beam as $\vec{S_1}$. We can see the Stokes parameters are a 4-vector that are, assuming no absorption, constrained to lie on the surface of a sphere. The output state of any optical component that modifies the polarisation of the light must also lie on the surface of the sphere. In other words, optical components perform rotations on the Stokes vector. Now, the change in polarisation of light due to transmission or reflection by an optical component, is – in Stokes vector convention – described by a Mueller matrix. These are named after Hans Mueller, who in 1943 discovered that any optical component can be characterised as a 4×4 matrix[15]. In general, the output polarisation for the light can be calculated as

$$\vec{S_1} = M \times \vec{S_0} \tag{2.7}$$

If more optical components, defined by M_1, M_2 etc. (in the order the light

[2]Provided the light is fully polarised. If the light is partially depolarised, $I^2 > P_1^2 + P_2^2 + P_3^2$. The difference between the left and right sides of the equation is equal to the amount of depolarised light.

[3]Taken over a period $\gg$ than the natural period of the wave, $\omega \sim 10^{15} s^{-1}$.

passes through them), are present, then

$$\vec{S_1} = M_2 \times (M_1 \times \vec{S_0}) \tag{2.8}$$

For example, a linear polariser that transmits only light linearly polarised at 45∘ with respect to the x-axis, has the following Mueller matrix

$$M = \begin{bmatrix} 1 & 0 & 1 & 0 \\ 0 & 0 & 0 & 0 \\ 1 & 0 & 1 & 0 \\ 0 & 0 & 0 & 0 \end{bmatrix} \tag{2.9}$$

Naturally, if the component has no effect on polarisation, $M = \mathbb{I}$ (the identity matrix). With this system, we are able to describe any polarisation of light, as well as the polarisation changes introduced by arbitrary optical components.

2.2 Ellipsometry

As mentioned in the introduction, as well as above, ellipsometry requires knowledge of the polarisation state. But what is ellipsometry, exactly? In short, ellipsometry compares the polarisation states of light before and after it reflects from the surface of a sample, and uses any difference to determine sample properties such as thickness and surface roughness. A simple schematic is presented in Figure 2.1. Light with a given polarisation state is reflected off a sample, and the change in polarisation state is measured.

We will briefly return to describing polarisation as in equations 2.1 and 2.2: as sinusoidal waves in the x- and y-directions. We will re-define these axes to mean light that is polarised *parallel* (p) and *perpendicular* (s) to the plane of incidence, also shown in Figure 2.1. Crucially, the sample has a different effect on p- and s-polarised light. The complex reflection coefficients for these two polarisation states are given by given by the Fresnel equations, also seen plotted (squared) as a function of angle of incidence in Fig 2.2:

$$r_p = \frac{n_2 \cos\theta_i - n_1 \cos\theta_t}{n_1 \cos\theta_t + n_2 \cos\theta_i} \tag{2.10}$$

$$r_s = \frac{n_1 \cos\theta_i - n_2 \cos\theta_t}{n_1 \cos\theta_i + n_2 \cos\theta_t} \tag{2.11}$$

with n_1 the refractive index of the medium, n_2 the refractive index of the sample, θ_i the angle of incidence and θ_t the angle of transmittance.

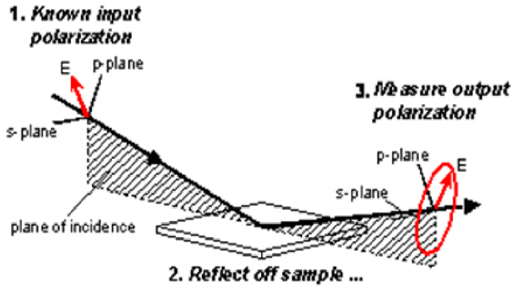

Figure 2.1: A basic ellipsometry measurement. Shown are the incident and reflected light beams and their respective polarisation properties, the sample, and the plane of incidence. Note that the polarisation state has gone from linear to elliptical after it is reflected from the sample. Source: J.A. Woollam CO online ellipsometry FAQ. Retrieved 8 June 2012.

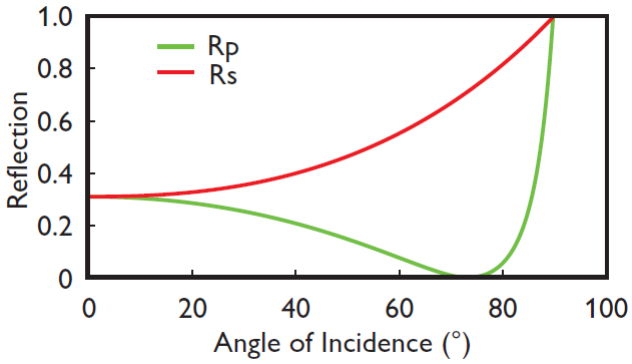

Figure 2.2: The reflection coefficients squared for p-polarised and s-polarised light, as a function of angle of incidence. $n_1 = 1$, $n_2 = 3.8$.

This model is detailed enough if light is reflected from a single interface. For thin films, which are of course the kind of samples we are interested in, the picture is slightly more complicated, since we have two interfaces to consider[4]: air/film, and film/substrate. For the moment, they will be referred to as $I1$ and $I2$, and we can define r'_p and r''_p, respectively by filling in the corresponding values for the air, film and substrate. It can then be shown that the full reflection coefficient for this sample is given by the Airy formula [16]

$$R_p = \frac{r'_p + r''_p exp(\imath 2\beta)}{1 + r'_p r''_p exp(\imath 2\beta)} \tag{2.12}$$

$$R_s = \frac{r'_s + r''_s exp(\imath 2\beta)}{1 + r'_s r''_s exp(\imath 2\beta)} \tag{2.13}$$

With β the phase shift between the top and the bottom of the thin film (second layer), given by the optical path difference between the two interfaces as $2\pi \frac{d}{\lambda} n_{film} \cos\theta$.

Since both r_p and r_s are complex numbers, the complex reflectance ratio can be expressed in polar form, with an amplitude ratio Ψ and a phase shift Δ

$$\rho = \frac{r_p}{r_s} = \tan\Psi e^{\imath\Delta} \tag{2.14}$$

We see, thus, that we generally need two parameters to define the light reflection from a sample: the ellipsometry parameters Ψ and Δ. In Mueller matrix form, this reflectance is defined as follows [16]:

$$M_s = \frac{\mid r_p \mid^2 + \mid r_s \mid^2}{2} \begin{bmatrix} 1 & -\cos(2\Psi) & 0 & 0 \\ -\cos(2\Psi) & 1 & 0 & 0 \\ 0 & 0 & \sin(2\Psi)\cos(\Delta) & \sin(2\Psi)\sin(\Delta) \\ 0 & 0 & -\sin(2\Psi)\sin(\Delta) & \sin(2\Psi)\cos(\Delta) \end{bmatrix} \tag{2.15}$$

Our goal is to build a full-fiber ellipsometer that enables us to measure Ψ and Δ.

[4] Of course, multilayer samples have more than two interfaces. These cases are generally more complicated, are and usually solved using transfer matrices [16].

2.3 Polarisation and ellipsometry

Now that we have succeeded in laying a mathematical foundation for light polarisation as well as introducing ellipsometry, the question of why Mueller matrices are used to describe polarisation states remains. It does not seem immediately obvious that this is a convenient system. The reason for using the Stokes formalism is that Stokes parameters can be measured directly[14], and, more importantly, easily. Compare Eqs. 2.3 - 2.6 to 2.1 and 2.2; it is much easier to measure intensity than it is to measure the amplitudes and phase differences of two waves. Another advantage of using Stokes vectors and Mueller matrices is that they deal with depolarising samples easier than other methods [14].

A typical polarimeter for the polarisation state in Stokes vector form, based on a rotating wave plate, a polariser and a photodetector, can be seen in Figure 2.3. The light passes through the wave plate, which modifies the polarisation based on its current position, and then through the polariser, after which the intensity of the light is measured. Since the polariser only transmits the portion of light parallel to the transmission axis, the intensity of the light is dependant on the position of the wave plate and the input polarisation of the light. Mapping the intensity for a full rotation of the wave plate then allows us to retrieve the original stokes vector (ie, S_1).

Since any optical component, including the samples that need to be measured, can be characterised by a 4×4 Mueller matrix, one would expect to need to measure 16 different parameters to fully determine sample properties. Fortunately, we can see from equation 2.7 that for isotropic, non-depolarising samples, measuring just two parameters (Ψ and Δ) is enough to (partially) characterise the sample. Characterisation is always partial, because sine and cosine are periodic functions, meaning that they will almost never produce a unique solution. This means that when performing ellipsometry at a single-wavelength and a single angle, an educated guess is usually necessary to obtain (for instance) the correct layer thickness. Measuring at multiple wavelengths eliminates this problem, as the wavelength-dependant Ψ and Δ functions will be different for different layer thicknesses, thereby solving the periodicity problem.

2.4 Fiber effect on polarisation

Now that we have dealt with polarisation theory, it is worthwhile to take a closer look at the effect of propagation through a fiber on the output polarisation. As explained in the introduction, fibers, in general, are non

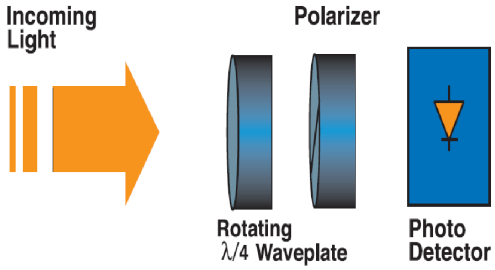

Figure 2.3: A schematic representation of a polarimeter using a rotating quarter-wave plate, a polariser and a photodetector. Source: Thorlab PAX5710VIS-T polarimeter schematics. Retrieved 11 December 2012.

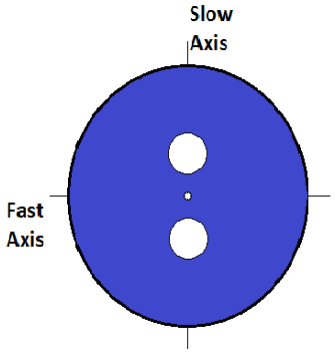

Figure 2.4: A crosscut of a Panda-style Polarisation-Maintaining Fiber. It shows the orthogonal fast and slow axes, as well as the core (middle) and stress rods (around the centre).

polarisation maintaining, meaning they will modify the Stokes vectors as given by the time-changing Mueller matrix of the fiber. To prevent this, polarisation-maintaining (PM) fibers were invented; a crosscut of such a fiber can be seen in Figure 2.4.

It can be seen that the PM-fiber has two main axes: a slow and a fast axis. These refer to the relative refractive indices for light polarised along these axes (recall the x and y axes from equations 2.1 and 2.2); the fast axis has a lower refractive index, resulting in a higher phase velocity for the component of the electric field oscillating along the fast axis, as the speed of light in a medium is given by $v_{light} = c/n$, with c the speed of light in vacuum and n the medium's refractive index. Light that is linearly

polarized along either the fast or slow axis of the fiber will remain so, because the projection of electric field is nonzero for only a single axis. In this case the light field will (in general) not, or minimally, couple from one mode to the other.[5] In the rest of this thesis, the fast and slow axes of the fiber are assumed to be parallel to the x and y axes, defined above, respectively. Nevertheless, in general, the light coupled into the fiber will have non-zero electric field components along both axes. Thus, light that is not strictly linearly polarised along either the fast or slow axis will be coupled into both modes, depending on the precise polarisation state when the light enters the fiber. Since the two modes do not couple, this means that the light is effectively coupled into two fibers: one carrying E_x, and one carrying E_y. However, since the component of the electric field oscillating along the fast axis travels faster, the phase difference between the two fields begins to sweep over the range of 0 to 2π. The length of fiber that causes enough retardation for the phase delay to equal 2π is called the *beat length*, $B(T)$. The beat length is given by the wavelength of the light and difference in refractive indices of the two fiber axes, or *birefringence*, as follows

$$B(T) = \frac{\lambda}{n_x - n_y} \tag{2.16}$$

This beat length is strongly temperature (and stress) dependant, meaning the fiber will usually not have a stable phase difference, or *retardation*. From the beat length, we can easily calculate the retardation through

$$\Omega_r = 2\pi \frac{L_f}{B(T)} \tag{2.17}$$

With L_f indicating the length of the fiber. Note that the polarisation state is fully defined by this phase difference and the amplitude of the beams (see equations 2.1 and 2.2) [14].

The question remains how to treat this fiber mathematically. It turns out we can treat an ideal fiber — that is, one that has no coupling between the x and y modes and has these axes perfectly aligned to the reference frame of the light — as a simple wave-plate [16]. This means the Mueller

[5] it is possible that light does couple between the fast and slow axis, due to the orientation of the fast and slow axis not being precisely orthogonal to each other over the length of the fiber. This effect is known as crosstalk, and was used by Liu to distinguish between light that had travelled the fiber once and light that had been through the fiber twice [13].

matrix M_F for a fiber depends only on the retardation (and thus the beat length), as follows

$$M_F(\Delta_r) = \begin{bmatrix} 1 & 0 & 0 & 0 \\ 0 & 1 & 0 & 0 \\ 0 & 0 & \cos\Omega_r & \sin\Omega_r \\ 0 & 0 & \sin\Omega_r & -\cos\Omega_r \end{bmatrix} \tag{2.18}$$

If the fiber axes are rotated with respect to the reference frame of the light, this results in a coordinate shift, given by the simple rotation matrix [16]

$$R(\alpha) = \begin{bmatrix} 1 & 0 & 0 & 0 \\ 0 & \cos 2\alpha & \sin 2\alpha & 0 \\ 0 & -\sin 2\alpha & \cos 2\alpha & 0 \\ 0 & 0 & 0 & 1 \end{bmatrix} \tag{2.19}$$

With *alpha* the angular difference between the reference frames of the light and the fiber. The full formula for describing the fiber's effects M_f then becomes

$$M_f = R(\alpha) \times M_F(\Omega_r) \times R(-\alpha) \tag{2.20}$$

Previous work by this group has shown that when light with a fixed polarisation is coupled into a fiber that is heated or cooled, and, therefore, has a continuously varying beat length, the output states form a fixed orbit on the Poincaré sphere [13]. This is due to the fiber only affecting the angle θ, defined in Eqs. 2.1 and 2.2, while the amplitude ratio of the two fields remains constant. More specifically, since only P_3 and P_4 are modified by the fiber, the orbit takes the shape of an ellipse in the 3^{rd} and 4^th Stokes vector-plane [6], and can, thus, be seen as a circle on the sphere. This circle is constant for any given input polarisation that remains constant relative to the reference frame of the fiber, meaning it will always produce the same output circle, provided the fiber's birefringence value varies enough to map it fully. Generally, changing the fiber temperature by about 3 or 4 degrees is enough to map a full rotation [17]. Crucially, this means the polarisation state of the light incident on the sample is known provided the fiber is pre-characterised; it must simply be treated as an collection of states rather than as a single point.

[6] We have ignored some small effects due to misalignment and production errors inside the fiber; these are treated in-depth in [17].

2.5 The half-fiber ellipsometer

The polarisation behaviour of both fibers and samples are now known; the question remains how to distinguish polarisation changes in one from polarisation changes in the other. Examining Eq. 2.15, it becomes clear that the effects for P_1 and P_2, and P_3 and P_4 can be treated separately since the sub-matrices of M_s are independent. Thus, Ψ and Δ can be treated separately.

Take I^{sp} as the set of Stokes vectors of light output by the fiber and incident on the sample and R^{sp} as the set of polarisation states of the light reflected from the sample. Then, in general,

$$R^{sp} = A \times M_s \times I^{sp} \tag{2.21}$$

Where we have assumed that all polarisation independent losses can be represented by a single loss-factor, A. Substituting

$$I^{sp} = \begin{bmatrix} I_1 \\ I_2 \\ I_3 \\ I_4 \end{bmatrix}, R^{sp} = \begin{bmatrix} R_1 \\ R_2 \\ R_3 \\ R_4 \end{bmatrix} \tag{2.22}$$

into equation 2.21 then gives the following set of equations:

$$R_1 = A(I_1 + I_2 \cos 2\Psi) \tag{2.23}$$
$$R_2 = A(I_2 - I_1 \cos 2\Psi) \tag{2.24}$$
$$R_3 = A \sin 2\Psi(I_3 \cos \Delta + I_4 \sin \Delta) \tag{2.25}$$
$$R_4 = A \sin 2\Psi(I_4 \cos \Delta - I_3 \sin \Delta) \tag{2.26}$$

Rearranging Eqs. 2.23 and 2.24 gives

$$R_1 = AI_1(1 + \cos^2 2\Psi) + R_2 \cos 2\Psi \tag{2.27}$$

This expresses a clear relation between R_1 and R_2 with the slope of the line given by $\cos(2\Psi)$. For Δ, note that Eqs. 2.25 and 2.26 consist of a scaling factor ($\sin(2\Psi)$, which is known) and a rotation based on Δ. The ellipses, created by plotting R_3 vs R_4 for I^{sp} and R^{sp}, will be rotated with respect to each other by the angle Δ.

The physics and resulting mathematical model, developed earlier will now be used to simulate the output polarisation states of two fibers in series with an arbitrary reference frame rotation between them—as might be

expected in any implementation of an all-fiber ellipsometer. These simulations will be used to guide experimental work and develop analysis tools to extract the ellipsometry parameters from measurement data.

3 Two-fiber simulation and mathematics

The work by Liu features extensive fiber modelling, focusing on crosstalk [17]. Such an approach requires careful simulation of internal fiber defects, resulting in a relatively complicated simulation. For our work, this is not required; a simple simulation of the polarisation output states from two successive ideal polarisation maintaining fibers, possibly with a sample in between, is enough. Thus, the fiber is treated simply as an ideal wave-plate with a Mueller matrix as seen in Equation 2.18. The full code for the fiber simulation can be found in Appendix B.

In short, the simulation consists of taking an input polarisation state (in Stokes vectors), and running this through a fiber with a varying beat length, resulting in some 1600 different output states. These are then used as input for a second fiber, which also has a (different) varying beat length. The resulting states are plotted on the Poincaré sphere. The fiber also has misalignment effects, as described in Eqs. 2.19 and 2.20. It is possible to add an optical element that affects the polarisation between these two fibers, thereby simulating a sample. Since the output polarisation states of the first fiber, sample, and second fiber are stored independently, it is easy to compare them and examine fiber and/or sample effects.

Before the simulation work is described, it is worthwhile to examine precisely what knowledge we hope to gain from doing simulations. The previous chapter has shown that for a half-fiber ellipsometer system, extracting Ψ and Δ is a mathematical process. How will this system change when a second fiber is introduced? Assuming, once again, that a fiber can be treated mathematically as a wave plate, the formula for the output of the second fiber F_{se} is given by

$$F_{se} = \begin{bmatrix} 1 & 0 & 0 & 0 \\ 0 & 1 & 0 & 0 \\ 0 & 0 & \sin 2\Psi \cos \Omega_r & \sin 2\Psi \sin \Omega_r \\ 0 & 0 & \sin 2\Psi \sin \Omega_r & -\sin 2\Psi \cos \Omega_r \end{bmatrix} \times \begin{bmatrix} R_1 \\ R_2 \\ R_3 \\ R_4 \end{bmatrix} \tag{3.1}$$

It is immediately apparent that the second fiber will not modify R_1 and R_2, which were used to measure Ψ in the half-fiber ellipsometer. Since these parameters are not modified, they can be extracted in the same way in the full-fiber ellipsometer. This means that only Δ remains to be determined, and the goal of the simulations is to assist in finding a way to extract Δ from the polarisation states output by a full-fiber system. Generally speaking, there are three approaches for dealing with the complications caused by the second fiber:

1. Stability: keep the fiber extremely stable, thus ensuring the polarisation change due to the fiber is always known during any particular measurement. This could be done by temperature controlling the entire length of the fiber, and keeping the fiber stress constant by careful positioning control. However, such a set-up is hard to realise in a conventional lab environment let alone an industrial environment. Still, it might be possible given the right type of fiber.

2. Compensating: constantly calibrate for fiber effects using fiber crosstalk, as explained by Liu [13]. The basic premise is that, since fiber-induced polarisation changes are linear, it is possible to map polarisation states of light that has travelled the length of the fiber twice to states of light that has travelled it once. This is possible because these states do not overlap: fiber crosstalk [7] causes a Lissajous figure to appear. Consequently, assuming the fiber can be kept stable over the course of the measurement, it would be possible to send a beam through the second fiber in the reverse direction, collect the light reflected from the end facet and use this to compensate for polarisation effects on the sample beam. This method has the disadvantage of increasing the complexity of the measurement setup; a way must be found to introduce polarised light into the end facet of the second fiber while still being able to perform polarisation measurements on light exiting the fiber at this end.

3. Understanding: although the pattern of polarisation states from the second fiber certainly appears to be random, the physics and mathematics behind it are quite well known and have deterministic features. Investigating the precise pattern might provide clues for uncovering the circle produced by the sample. In short, the problem would be tackled mathematically.

Maintaining the fiber in a stable state was deemed too impractical to test in the laboratory, as controlling fiber stress and particularly temperature would be very difficult in any practical sense. One interesting development for this approach may be that researchers have recently succeeded in making a specific kind of fiber completely temperature-independent at a specific wavelength [18], making it extremely stable – although the fiber will, of course, still be susceptible to external stresses. Nevertheless, if it is possible to construct temperature-independent fibers at desired wavelengths,

[7] Explained in more detail in Section 2.4

this is certainly promising for fiber ellipsometry as it significantly reduces the work required for stabilising the fiber. For now, this approach is still too impractical for our purposes. Considering the two remaining options, attempting to understand fiber behaviour seems to be the most elegant solution, and it is one that lends itself to simulations very well. Thus, the goal of the simulations is to shed more light on the polarisation behaviour of a full-fiber system: in particular, how Δ can be deconvolved from the polarisation states of light exiting the second fiber.

3.1 Characteristic circles and bands

Previous work has shown that polarisation-maintaining fibers project incoming polarisation states into characteristic circles on the Poincaré sphere. The orientation of these circles depends on fiber misalignment and input polarisation only; rate of beat length change and other factors play no role – these only decide to which part of the circle the input state is mapped. Thus, since fiber misalignment is typically constant, these circles will, in theory, only be modified by the input polarisation state. This can be seen in the Fig. 3.1, where, in our simulation, different possible input polarisations (shown in purple) resulted in different circles on the sphere (shown in (light) blue, red and green). Note that these circles appear to be parallel to each other. Mathematically, this can understood by examining Eq. 2.20. Since the fiber only modifies the third and fourth Stokes parameters, the output circle can be expected to lie along the axis of the second Stokes parameter. This axis is rotated by misalignment between the axis of birefringence of the fiber and the measurement basis of the polarimeter, resulting in the orientation seen in the figure.

Fig. 3.1 shows one more interesting characteristic. Taking a close look, we can see that the possible output states are limited by the input states. If the input states consist of a circle that is not a great circle and the circles formed by the polarisation states output from the second fiber are not orthogonal to the input circle, or if the input state is not a great circle, *it is not possible to map every point on the sphere*! Rather, (assuming all possible output states are mapped), the pattern forms a band on the sphere with the *position* determined by the input circle, and the *direction and maximum width* determined by the orientation of the input circle and the second fiber's characteristic circles.

In order to test what happens when the input polarisation states for a fiber vary during the experiment, a more accurate representation of the fiber ellipsometer was simulated. This simulation used a constant input

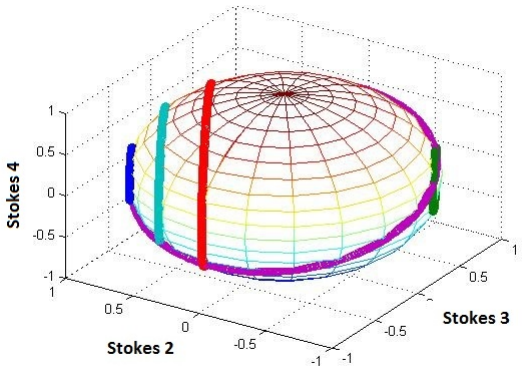

Figure 3.1: A simulation of output circles from a modified polarisation-maintaining fiber mapped on the Poincaré sphere. Possible input states shown in purple; output states shown in (light) blue, red and green. The output states are parallel to each other, and map a full circle. One of the implications of this is that every output circle will cross the circle of input polarisation states precisely twice except in edge cases.

polarisation state for the first fiber, which had a constantly changing beat length, and used the output states as input for a constantly changing second fiber, which had a different beat length. For these simulations, two fibers of length 2 m were considered. Both fibers had a starting beat length of 1.8 mm, but different temperature dependence. The beat length varied by 1% in the first fiber and 1.1% in the second fiber. Relative to the laboratory coordinate system, the coordinate system of the first fiber was rotated by $\frac{1}{4}\pi$, and the second by $\frac{1}{8}\pi$. The input polarisation state was set to be circularly polarised light. The result is shown in Fig. 3.2, with the output states of the second fiber shown in blue and the output circle of the first fiber in green. The band structure predicted by our simple simulation is evident, and, as predicted by our earlier simulations, the width and position of the band are determined by the first fiber's output states. The band is not completely filled because the simulation was not run for a sufficient period of time.

So, what does this all mean for the fiber ellipsometer? The simulation and mathematics indicate that inputting a range of different, adjacent, polarisation states will result in a band on the Poincaré sphere as output from the second fiber. Since this band is at least partially characterised by the input circle – meaning here the polarisation states off the light reflected from the sample – an attempt could be made to use this band to deconvolute the

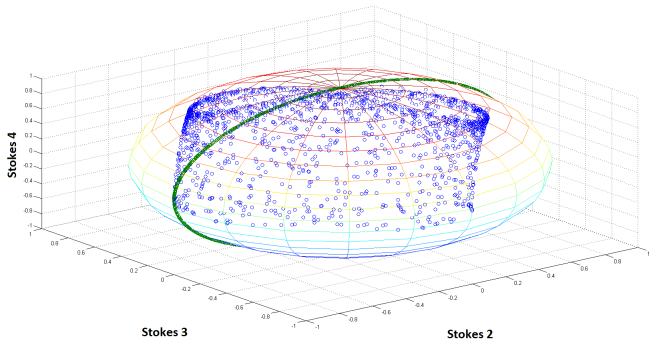

Figure 3.2: Simulated output polarisation states for two successive polarisation-maintaining fibers. Output states of the second fiber are shown in blue; the collection of output states of the first fiber are imposed in green. The output can clearly be described as a band on the Poincaré sphere, and the width and location is indeed determined by the first fiber's characteristic circle of output states.

original signal. However, care must be taken: with our understanding now, it seems that the band seen on the sphere can be generated by any number of different input circles, as several axes of symmetry can be identified. For instance, the circle shown in Fig. 3.2, can be rotated either closer to or further away from the top of the sphere without changing the output circle. It can also be mirrored in the 'centre axis' of the band. This means that any solution to obtain Δ using this band will be insensitive to a number of different operations. Therefore, it is worthwhile to investigate how, precisely, Ψ and Δ influence this band signal.

3.2 Psi

We have noted in Sec. 3 that the second fiber will most likely not affect the method for extracting Ψ from the data. However, it is still worthwhile to see how it will influence to band structure. Ignoring the resizing effect on the third and fourth Stokes vectors (as these are normalised anyway), Ψ has the following Mueller matrix:

$$M(\Psi) = \begin{bmatrix} 1 & -\cos 2\Psi & 0 & 0 \\ -\cos 2\Psi & 1 & 0 & 0 \\ 0 & 0 & 1 & 0 \\ 0 & 0 & 0 & 1 \end{bmatrix} \tag{3.2}$$

Thus, Ψ influences only the first Stokes vector, which is the total intensity of the light, and the second Stokes vector – the amount of light that is linearly polarised. Assuming $S_1 = 1$, after reflection from the sample S_2 will be equal to $S_2 - \cos 2\Psi$. This means that the sample's output circle will be shifted along the second Stokes vector by a factor 2Ψ. In terms of the band structure, this means the band will shift with it. Taking the centre of the Poincaré sphere as a reference point, as an ideally aligned system will have this as the centre point of the circle of polarisation states used as the probing state, Ψ is given by

$$\Psi = \frac{\arccos x_1}{2}, \tag{3.3}$$

with x_1 the x-position of the centre of the band.

3.3 Delta

It has already been noted by Liu that the effect of Δ is that of a rotation of the third and fourth Stokes vectors. In Mueller matrix form, this is identical to the matrix for a clockwise rotation (assuming Δ is positive)

$$M(\Delta) = \begin{bmatrix} 1 & 0 & 0 & 0 \\ 0 & 1 & 0 & 0 \\ 0 & 0 & \cos\Delta & \sin\Delta \\ 0 & 0 & -\sin\Delta & \cos\Delta \end{bmatrix} \tag{3.4}$$

Rotations always have two key characteristics: the angle of rotation and the axis of rotation. Here, it is obvious Δ is the angle of rotation. We can see from Eq. 3.4 that in this case, the axis of rotation is the first Stokes vector. The rotation matrix is such that an input state and rotation angle always map to a unique output state. On the face of it, though, it would appear that given input and output states, a unique rotation angle cannot be determined because $\cos\Delta = \cos(2\pi - \Delta)$. However, the coordinate system that we use requires $0 \leq \Delta \leq \pi$, so, the rotation angle can be uniquely determined from input and output states

We return now to the situation of our fiber ellipsometer. We know that rotation matrices will always give unique output states. Working with circles on a sphere, these states can be defined by two things: the location of the circle centre and the circle's orientation. Note that we do not need to define the radius, as this will be held fixed by the Poincaré sphere. Also note that, since we are only considering rotations around the second Stokes vector, the circle's orientation is fully given by the angle it makes with either the

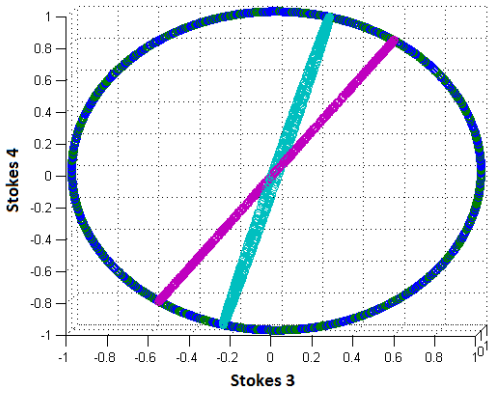

Figure 3.3: Simulated data to show the effect of different delta values. Data in purple has $\Psi = 45\,\text{deg}, \Delta = 15\,\text{deg}$; data in light blue has $\Psi = 45\,\text{deg}, \Delta = 35\,\text{deg}$. The characteristic circle of a perfectly aligned fiber is added in dark blue. It is clear that the rotation due to Δ is centred around the second Stokes vector.

third or fourth Stokes vector, which of course is related to Δ. In any case, this means that if we can define the circle centre and orientation, we have uniquely identified it.

So, what does Δ do in terms of band characteristics? It has been noted in Section 3 that – disregarding all fiber misalignment, and ignoring Ψ – the characteristic circles of a fiber lie parallel to the second Stokes vector. In other words, the band from a perfectly aligned fiber will lie precisely orthogonal to any changes (i.e., rotations) in the polarisation state after reflection off the sample! Thus, when dealing with a perfectly aligned system[8], changes in Δ will not show in the output band! This effect can be seen in Figs. 3.3 and 3.4, which were created using the same simulations described above, but with misalignment set at 0 deg and Ψ at 45 deg. The first image shows a rotation in the sample circle due to a different Δ value; the difference between the two circles is 20 deg. Fig. 3.4 shows the same two circles from a different perspective. In both images, the direction of a perfectly aligned fiber's circle added in dark blue. Since this circle is orthogonal to the axis of rotation, changes in Δ will not appear in the output band.

So, how to solve this issue? The answer lies in misalignment. Fiber misalignment will result in the light being rotated into the reference frame

[8] And, again, ignoring all effects caused by Ψ

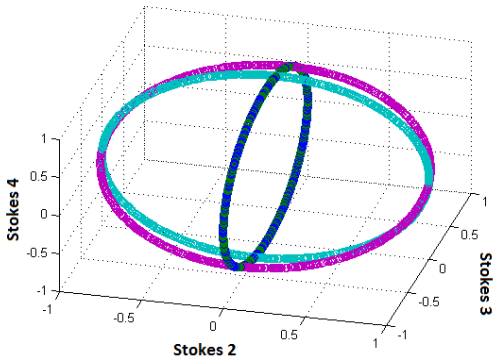

Figure 3.4: Simulated data to show the effect of different delta values. Data in purple has $\Psi = 45\,\text{deg}, \Delta = 15\,\text{deg}$; data in light blue has $\Psi = 45\,\text{deg}, \Delta = 35\,\text{deg}$. The characteristic circle of a perfectly aligned fiber is added in dark blue. It is clear that this characteristic circle is orthogonal to the axis of rotation, meaning these rotations will not show in the output band.

of the fiber via a rotation matrix

$$M(\alpha) = \begin{bmatrix} 1 & 0 & 0 & 0 \\ 0 & \cos 2\alpha & \sin 2\alpha & 0 \\ 0 & -\sin 2\alpha & \cos 2\alpha & 0 \\ 0 & 0 & 0 & 1 \end{bmatrix} \tag{3.5}$$

Where α is the misalignment of the fiber's reference frame with that of the sample (the $x - y$ axes). At the back end of the fiber, the rotation is in the opposite direction, meaning the data must be multiplied by the inverse of the matrix shown above. This means that at a front misalignment angle of $\alpha = 45\,\text{deg}$, horizontally polarised light effectively becomes 45 deg polarised and vice versa. Thus, rather than changes in Δ causing a rotation in the 3-4 Stokes vector plane, they now cause a rotation in the 2-4 plane, which is no longer orthogonal to fiber's characteristic circle! This is demonstrated in Figure 3.5.

Then, a different angle Δ results in a different band width, and the angle change Δ can be calculated from

$$\Delta = \arcsin \frac{w_1}{2} - \arcsin \frac{w_0}{2} \tag{3.6}$$

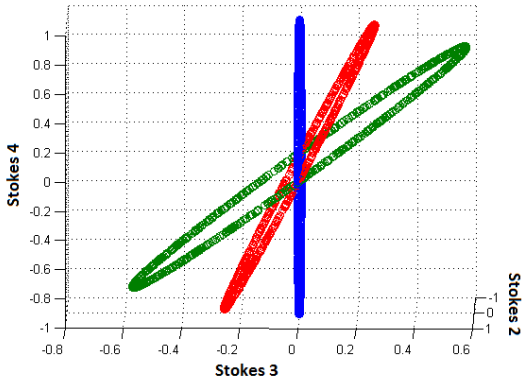

Figure 3.5: Simulated data to show the effect of different delta values, shown in the same projection as in Fig 3.3. Data in red has $\Psi = 45\,\text{deg}, \Delta = 15\,\text{deg}$; data in green has $\Psi = 45\,\text{deg}, \Delta = 35\,\text{deg}$. The characteristic circle of fiber that is misaligned by 45 deg is added in dark blue. It is clear that this characteristic circle is now parallel to the axis of rotation, meaning these rotations will show have an effect on the output band.

With w_0 the original full band width, and w_1 the new band width. One question remains: have we solved the problem uniquely? Unfortunately, the answer is no. After all, $\sin(x)$ is symmetric around 90 deg, meaning that our formula will nearly always give two solutions: Δ and $180 - \Delta$. However, provided we have some information about the sample and stay away from $\Delta \approx 90\,\text{deg}$, Δ should be uniquely solvable. Furthermore, since Δ will vary at different angles of incidence, measuring at different AOI will generally result in different results for Δ, which will most likely not all lie very close to the point of symmetry, simplifying the analysis process.

This method will also work for misalignment angles that are not precisely equal to 45 deg, although smaller or larger angles will cause the changes in Δ to become less pronounced.

3.4 Deconvolving Psi and Delta from the band

What would this method look like in practice? Obviously, it is important to accurately determine band width. Consider that any circle on the Poincaré sphere can be defined as the collection of points of intersection of a plane in 3D space with the sphere. In other words, rather than having a parametric

equation for the circle, the characteristic circle can be defined in Cartesian coordinates as

$$P(\theta, \phi) = a_i x + b_i y + c_i z + d_1 \tag{3.7}$$

With $P(\theta, \phi)$ representing all points on the Poincaré sphere, a_{i1}, b_i and c_i defining the orientation of the plane[9], and d_i giving the position of the circle on the sphere. This means that determining a fiber's characteristic circle does not have to be done by a complicated fitting of parametric equations in 3D space, but can simply be done by least-squares fitting a plane to the collected data points. Following this, once the orientation of the circle (meaning parameters a_i, b_i and c_i) is accurately known, any subsequent circle fitting for this fiber is reduced to a one-parameter fit of d_1. This means that output circles can be fit very accurately, as there are no dependant variables.

This, in turn, means that the two circles at the edges of the band pattern obtained from the second fiber can be fit with high precision, giving us both circles' positions on the sphere (note that, since circle orientation is known, this also gives their radius). These positions will be defined as C_1 and C_2 respectively. Note that, because of symmetry arguments, the centre of the band will always be in the middle point between the centres of the two edge circles. With this centre known, it is trivial to calculate Ψ. Of course, this value for Ψ can always be checked against the value obtained through the intensity method, as used in the half-fiber ellipsometer. C_1 and C_2 also give the width of the band simply as the distance between these parallel planes. As can be seen above, provided the misalignment angles are known, this gives enough information to calculate Δ.

[9]Recall that, since the output circles are parallel, these values will be characteristic and, more importantly, constant, for a given fiber.

4 Fiber experiments

As we have seen in Section 3, two polarisation-maintaining fibers in a row will, most likely, produce an output series of polarisation states that resembles a 'band' on the Poincaré sphere. It seems that placing a second fiber after the first one (and possibly also after a sample) results in the output circle being mapped to the second fiber's characteristic circle on the Poincaré sphere. If this is indeed the case, it seems it will be possible to obtain Ψ and Δ from this band. Of course, the question remains as to whether this phenomenon is actually seen when using real fibers. The remainder of this section will show experimental results and analysis of polarisation measurements done first, on two successive PM fibers, then after adding a rotatable quarter-wave plate between them, and, finally, using the setup (without the intervening waveplate) for a series of ellipsometry measurements, performed on silicon wafers with varying thicknesses of silicon oxide.

4.1 Experimental setup

The basic measurement setup for these experiments can be seen in Figure 4.1. In short, it consists of a light source (HeNe laser, wavelength: 632.8 nm, output power: 5 mW), a Wollaston prism that sets the initial polarisation to linearly polarized light with a purity of 100000:1, and a quarter-wave plate to adjust the input polarisation state of the light. After polarisation control, the light is coupled into the first PM fiber (with coupling lenses), and recollimated on output. Between the first and the second PM fibers, a rotatable quarter-wave plate (not present in the initial measurements), and a non-polarising beamsplitter were placed. The ~~light~~ collimated output from the second fiber was directed to a polarimeter for measurement. The light reflected from the non-polarizing beamsplitter was directed to a second polarimeter, allowing the polarisation state of the light from the first PM fiber and quarter-wave plate to be measured simultaneously with the polarisation state of the light from the second polarimeter. In later experiments, the quarter-wave plate between the fibers was replaced with a sample holder, on which different samples could be mounted. This meant the setup had to be repositioned to allow reflection off the sample. For these measurements, the angle of incidence was held constant by the constraint that the light had to successfully couple into the second fiber, which has a MFD of 4.5 μm. Since the fiber lens has a focal length f of 11 mm, and the distance d from the lens to the sample was approximately 37 cm, the maximum angular uncertainty is 2.25 $10^{-6}/(d+f)$, or approximately 0.0003 deg. The angle of

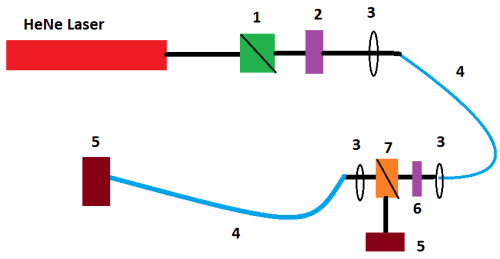

Figure 4.1: A schematic representation of the measurement setup used for fiber testing. Optical components consist of (1) a Wollaston prism, (2) a quarter-wave plate, (3) coupling lenses, (4) Polarisation-maintaining fibers, (5) a Thorlabs polarimeter, (6) a rotatable quarter-wave plate (not present in the initial experiments) and (7) a non-polarising beamsplitter. Note that the second fiber does not have an output coupling lens, as it is connected directly to a lens in the polarimeter.

incidence was determined to be 44.5 ± 0.5 deg.

To modify the fibers, they were both wrapped around a stainless steel tube, which was heated using a Braun Silencio 1250 hair dryer that was placed in the opening. Parts of the fiber that were not wrapped were left unsecured on the bench. Polarisation measurements were performed using the Thorlabs PAX5710VIS-T polarimeter, which operates in the $400 - 700$ nm wavelength range. It has a maximum sample collection speed of 330 samples/second, and the maximum number of data points that can be collected in one measurement series is 1024. Unless noted otherwise, 30 ± 1 microWatts of circularly polarised light was coupled into the first fiber and measurements were performed over 60 seconds, during which the fibers were continually heated. Sample interval was 60 ms. Due to the delay in heat transfer, the rate of fiber modification in the first moments after turning on the hair dryer was still quite low, possible preventing us from mapping the full circle on the Poincaré sphere. Thus, for each measurement, a 15-second warmup time was held during which the tube was heated, but no data was collected yet.

4.2 Polarisation effects of two successive PM fibers

To check whether the band structure introduced in Section 3 does indeed appear, a very simple initial experiment was performed: two fibers were placed in sequence, and the output polarisation was measured. These par-

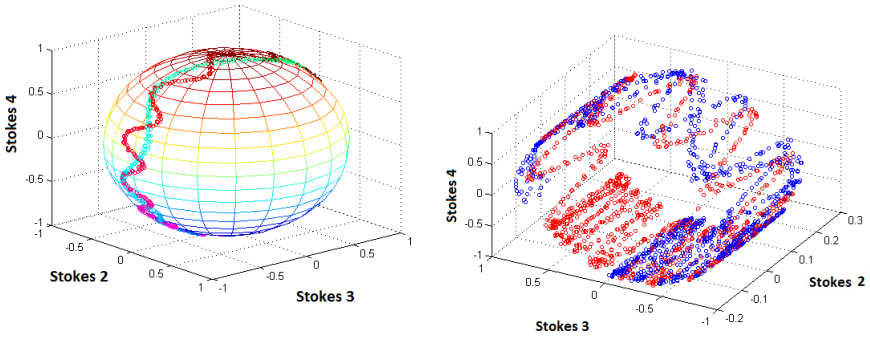

(a) Polarisation data from two sequential PM fibers. Colourscale changes from black to green as the measurement progresses. A clear band on the sphere - albeit not fully mapped - can be seen. Note that the periodicity of the smaller, sinusoidal pattern in the data changes as the measurement goes on, and that the signal has a 'reflection point' at the bottom of the graph.

(b) Polarisation data from two sequential PM fibers, collected on two different days. Red datapoints show one day, blue the other. The patterns share the same width and orientation, although they do not share the same reflection point. Sphere not plotted to reduce graph clutter.

Figure 4.2: Polarisation data from the second fiber, collected using Thorlabs polarimeter. Data was collected every 30 ms for a little over 30s.

ticular experiments were done with a sample interval of 30 ms, for a total measurement time of a little over 30 seconds. All other experimental conditions were the same as those indicated in Section 4.1. The resulting Stokes vectors can be seen in Figure 4.2 (a). (b) Shows data for the two wrapped fibers collected on different days.

In these figures, two main patterns can be identified: a circle around the Poincaré sphere, and a sinusoidal pattern around this main circle. To test which pattern is caused by which fiber, the experiment was repeated with only the first fiber wrapped. The result can be seen in Fig. 4.3. It is clear that the fast modulation, the 'baseline circle,' as it were, is caused by the rapidly modified first fiber, while deviations are caused by the unmodified (but still changing) second fiber. Modifying both fibers results in the clear band seen in Fig. 4.2 (a).

These experiments show exactly what we suspected: a band on the Poincaré sphere. The first fiber determines the band's baseline position,

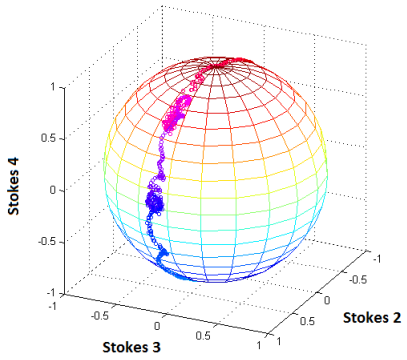

Figure 4.3: Polarisation data from the second fiber, collected using Thorlabs polarimeter and plotted on the Poincaré sphere. Data was collected every 30 ms for a little over 30s. Only the first fiber was modified. These results indicate that the fast movement around the sphere is caused by the first fiber, with the second fiber giving deviations with a fixed maximum width.

and orientation of the two fiber's characteristic circles determines the width and orientation of the band. Note that the periodicity of the second fiber's modifications changes as the measurement goes on (the colour scale goes from black to green, with a reflection point). This is likely caused by the steel tube heating slower as the experiment progresses, causing a slower beat length modification. What causes the reflection point is not quite clear; it seems like the direction of rotation for the mapping of the first fiber's circle suddenly reverses when reaching a certain point. Apparently, it is not a constant effect, as measurements taken on different days show different reflection points. Since the reflection point does not seem to obstruct characterisation of the band structure, it was not further investigated. Finally, note that band width in measurements done on two different days is identical, as shown in Fig. 4.2 (b). Thus, the band width and orientation are truly fixed values, dependant on the precise measurement setup. This, of course, means the setup can be calibrated. With the physical intuition gained from the simulations confirmed, we can now attempt to modify the signal coupled into the second stage of our ellipsometer by introducing an optical element between the first and second fiber.

4.3 Quarter-wave plate experiments

To test if misalignment effects can indeed be used to map one Stokes parameter on the other, a quarter-waveplate was used, as it has a Mueller matrix similar to that of a misaligned piece of PM fiber, as can be seen in Eq. 4.1. Mounting a quarter-wave plate in a rotation stage is easier than fitting such as stage to the precise positioning equipment used to couple the second fiber. The goal here will be to check whether it is indeed possible to influence the width of the output signal by varying the quarter-wave plate's misalignment angle θ.

$$M_{\frac{1}{4}\lambda}(\theta) = \begin{bmatrix} 1 & 0 & 0 & 0 \\ 0 & \cos^2 2\theta & -\cos 2\theta \sin 2\theta & 0 \\ 0 & -\cos 2\theta \sin 2\theta & \sin^2 2\theta & 0 \\ 0 & 0 & 0 & 0 \end{bmatrix} \tag{4.1}$$

Tests with the quarter-wave plate were done with the wave plate at a number of different angles, varying from 0 to 45 degrees. These angles do not correspond to an actual value for θ, but correspond to some reference angle. Values for 10 and 20 degrees (superimposed in red) are shown in Fig. 4.4, below. A big difference in band width can be seen right away. A plot of band width versus wave plate angle can be seen in Fig. 4.5 (line inserted to guide the eye). Band width was determined by finding maximum and minimum values for the second Stokes vector at constant S_3. The size of the projection of S_3 on S_2 clearly varies with wave plate angle, reaching a minimum at 25 deg before rising again, suggesting a periodic nature. This fits excellently with our understanding of the two-fiber system and the role of misalignment effects. For a perfectly aligned system, the minimum band width should be (close to) zero; the fact that we do not see this is an indication that our fibers are not aligned very well.

With our understanding of the fiber mathematics experimentally confirmed once again, we may now attempt to do measurements on 'real' samples and attempt to extract Ψ and Δ from them.

4.4 Silicon wafer experiments

In order to rigorously test the fiber ellipsometer and the behaviour of a 2-fiber system, reference samples were needed; that is, samples where ellipsometry measurements can be compared to those done with a commercial ellipsometer. Silicon wafers are ideal for this; they are flat and, thus, easily measurable, and untreated wafers are – for our purposes – identical to each

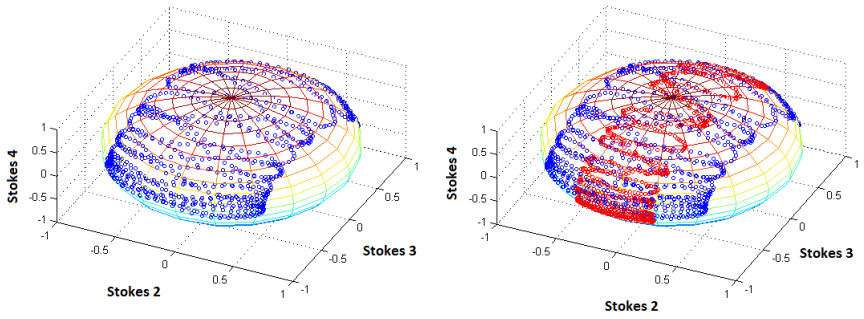

Figure 4.4: Figures (a) and (b) show polarisation data taken with a quarter-wave plate placed between the two fibers. (a) Has the wave plate at 10 degrees, (b) has the data for 10 degrees in blue and 20 degrees in red. It is immediately clear that there is a big difference in the width for the two bands, although the orientation of the bands does not same to change for different wave plate angles.

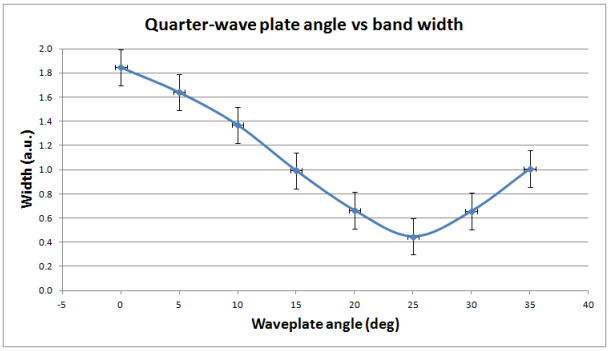

Figure 4.5: A plot of band width for rotation angles of the quarter-wave plate. The periodic nature of the data suggests our understanding of misalignment effects is correct.

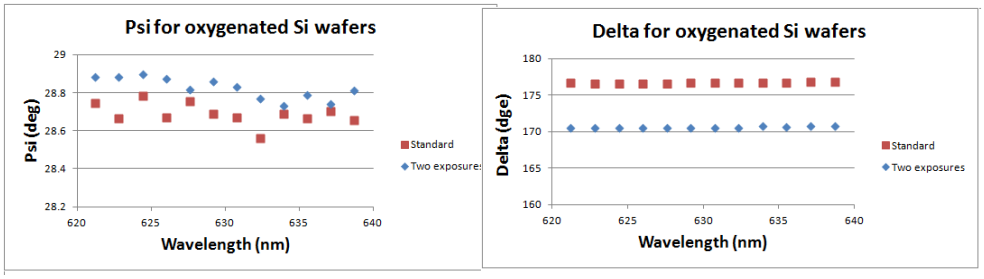

Figure 4.6: Figures (a) and (b) show ellipsometry measurements done on regular silicon wafers, as well as data collected from samples that have been exposed to oxygen plasma once and twice. For both Ψ and Δ, a clear shift can be seen, but note the different scale bars for the two graphs. Measurements done using Woollam M-2000 ellipsometer at an AOI of 55 deg.

other, so that performing reference measurements is simple. In order to obtain different samples, silicon wafers were exposed to an oxygen plasma for several minutes either once or twice. After oxidation, the wafers were re-characterised using a Woollam M-2000 Ellipsometer at an angle of incidence of 55 deg. Note that the precise oxidation time is irrelevant: the main goal is for the samples to be different from each other, but constant in time. Silicon oxide on silicon wafers meets these requirements.

Characterisation of the exposed samples in the Woollam reveals a clear change in Ψ and Δ values, as evidenced in Fig. 4.6. Unfortunately, there was no data collected for the once-exposed sample at this AOI. Data obtained at different AOI shows Δ values lying between the other two samples. Note that this graph shows only the wavelength range that is relevant for our HeNe fiber ellipsometer, and note also the different ranges on the y-axis for the two graphs. In any case, it is clear that Δ shifts by nearly 7 degrees between the three different silicon wafers. Since the fiber ellipsometer has an angle of incidence of 44.5 deg, the difference in Δ is expected to be smaller than the values found in the Woollam[10], but should still be observable for our system. The shift in Ψ is smaller still, but can nevertheless easily be detected using the Woollam.

Unfortunately, this is not the case for the measurements done by the Fiber ellipsometer. Fig. 4.7 shows data collected for the standard (a), once-treated (b) and twice-treated (c) silicon wafer. The combined datasets can

[10] As can, for example, be seen in Fig. 2.2

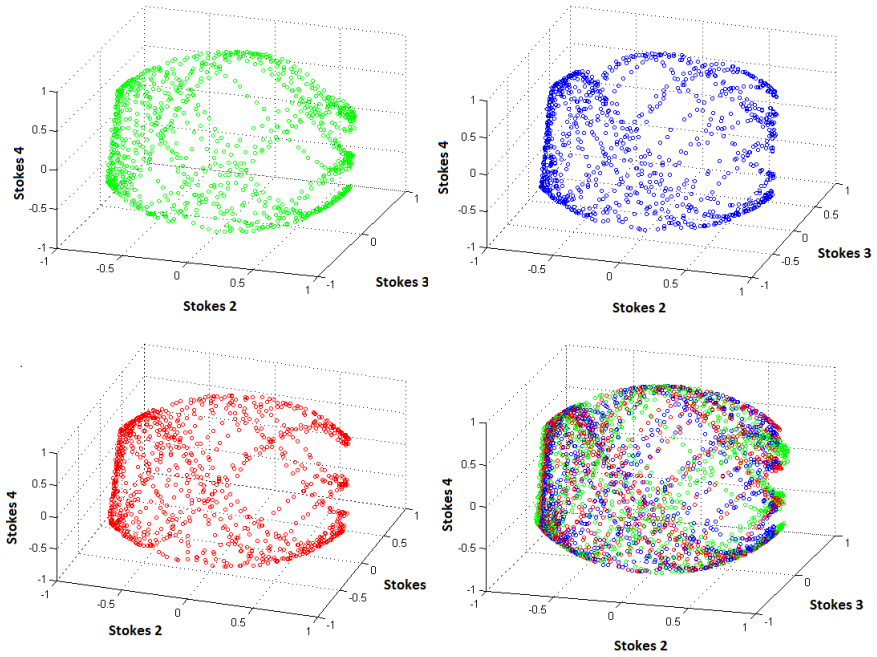

Figure 4.7: Figures (a), (b), (c) and (d) show fiber ellipsometry measurements done on regular silicon wafers, as well as data collected from samples that have been exposed to oxygen plasma once and twice. A standard wafer is shown in (a), once-treated in (b), and a twice-treated silicon wafer is shown in (c). The combined datasets can be seen in (d).There is no clear visible shift in band width or position.

be seen in (d). Measurements were done with both fibers wrapped, heated for 60 seconds. After each measurement series, the fiber ellipsometer was re-aligned by slightly adjusting the sample holder. As mentioned above, this does not change the angle of incidence, as fiber coupling constraints demands the AOI to be constant.

The data, albeit messy, shows no clear width discrepancy for the different samples, even though this should occur according to our understanding of the fiber mathematics. There could be several reasons for this:

- Our understanding of the mathematics may be wrong. This seems unlikely, as the calculations were confirmed by the experiments done in Section 4.2. Still, it must be pointed out that mathematically speaking, a wave plate is quite a bit different from a sample, and so we will

not necessarily see the same effects for a sample as for the wave plate.

- The changes in Ψ and Δ might be too small to be detected using the fiber ellipsometer. Ψ shows as a shift in the centre position of the band; the rotation due to Δ in the band width as a function of the misalignment angle. Both the changes in Δ and Ψ are quite small, and might simply be insensitive to them, especially at this angle of incidence.

- Even though the sample ellipse might be rotated and resized, this does not necessarily show in the output from the second fiber. For instance, if the ellipse is rotated 180 degrees around an axis parallel or orthogonal to the second fiber's characteristic circle on the sphere, this will not show in the output band. Such an in-plane-rotation effect might be in play here. Another possibility is that the non-polarising beamsplitter, being an optically active element, is wreaking havoc with the output polarisation states.

Of these possibilities, the second seems the most likely. We have not attempted to maximise the projection of the third Stokes onto the second one by the misalignment effects; therefore, an already small change in Ψ and Δ will most likely be made smaller still because the third Stokes vector is not fully projected. Furthermore, consider that, at the values measured for Δ in the Woollam, we would expect a very small band output from our fiber ellipsometer, as Δ is close to 180 deg. However, we instead get a very broad band, suggesting that the non-polarising beamsplitter in between the sample and second fiber might have a significant effect on the polarisation state. Even though this effect can be compensated for, it is highly undesirable, since it further obfuscates changes in the polarisation state caused by the sample. Taken together, it seems that testing the fiber-ellipsometer's functioning in this setup is doomed to fail, and this shows that it is perhaps too early to think of characterising samples using this system. We do, however, still require a proof-of-concept.

4.5 Proof of concept

At its most basic, what needs to be demonstrated to prove our understanding of the full-fiber system is that the polarisation state(s) of the light after the sample can be linked to those after the second fiber. If we can show the output band from the second fiber is indeed limited by the polarisation state directly after the sample, and if we can demonstrate that – when

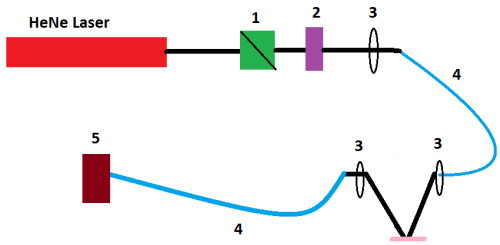

Figure 4.8: A schematic representation of the measurement setup used for fiber testing. Optical components consist of (1) a Wollaston prism, (2) a quarter-wave plate, (3) coupling lenses, (4) Polarisation-maintaining fibers, and (5) a Thorlabs polarimeter. Note that the second fiber does not have an output coupling lens, as it is connected directly to a lens in the polarimeter.

compensating for misalignment – we have proven that Ψ and especially Δ can be deconvolved from a two-fiber system. For this, it will be necessary to measure the polarisation state of light directly after a sample as well as after the second fiber. However, as noted above, we want to avoid using the non-polarising beamsplitter, as it complicated the setup (and analysis) by introducing an additional optically active element. In order to measure the sample circle, space was left open between the sample and the coupling stage of the second fiber, so that a polarimeter could be placed there. A similar tactic was used for measuring light exiting the first fiber. Other setup details were identical to those in Sec. 4. The setup can be seen in Fig. 4.8. To collect more data from the second fiber, 10 sets of 1024 data points each were collected over approximately 7 minutes as the fiber was cooling. Otherwise, the measurement procedure was identical to one described above.

4.6 Setup characterisation

As can be seen above, fiber misalignment is crucial both for correctly understanding and for correctly interpreting the results. Misalignment was measured by inputting linearly polarised light into the fiber, aligned to either the slow or the fast axis, which is when modification of the fiber has the least effect on the output polarisation state[11]. It was then checked at which

[11] Theoretically, if light is coupled into a single axis, modification should have no effect as all. However, crosstalk will always cause a small change in polarisation.

angle to the second Stokes vector - seen in the reference frame of the polarimeter – the linearly polarized was entering the detector.[12] This was done over a time of 30 seconds, and the resulting values were averaged. At the sample end, the fiber was misaligned by 3.8 ± 0.4 deg, and at the polarimeter end by 9.5 ± 1.0 deg. This method does not show, however, if this misalignment angle should be compared to the second or third Stokes vector (seen from the perspective of the fiber). As mentioned in Sec. 3, an extra misalignment angle, ideally of 45 deg ± 90 deg, is required to obtain usable data. Fortunately, our measurements indeed show this misalignment angle, meaning that the front misalignment angle is actually -45 deg $+3.8$ deg. Now, in order to equalise the reference frames, all data taken before the light enters the second fiber must be multiplied by $M(\alpha)$, with $\alpha = 48.8$ and all measurements collected after the second fiber by $M(\alpha)^{-1}$, with $\alpha = 9.5$. If the sample circle and the output band match up after these transformations, and if we can show that a different sample circle would result in a different band, we have our proof-of-concept.

4.7 Results

Measurements were done on two of the samples also used above: the reference wafer and the twice-exposed wafer[13]. Figure 4.9 shows first the non-standardised measurements for the unexposed wafer, with the sample circle in blue and the output band in green. It is clear that they do not match up in the slightest. In Fig. 4.10, the characteristic band of the second fiber (also not equalised, but in the same frame of reference as the output band) is plotted. Note that the edges of the band and the orientation of the characteristic circle match up. Finally, the rotated polarisation states, now in the same frame of reference, are plotted in Fig. 4.11. The width of the band and the orientation of the sample circle match up! The measurements for the twice-exposed wafer, in identical frames of reference, can be seen in Fig. 4.12. Again, the width of the band and the orientation of the sample circle match. Finally, Fig. 4.13 displays the two different sample circles, reference in blue, twice exposed in red, showing that indeed the difference in orientation between the two circles is very small.[14] The difference in Δ was determined to be 6.9 deg, agreeing with the values found in the Woollam.

[12] This is the *azimuth* angle.

[13] For obvious reasons, the once-exposed wafer was no longer available

[14] This is effectively a half-fiber ellipsometer.

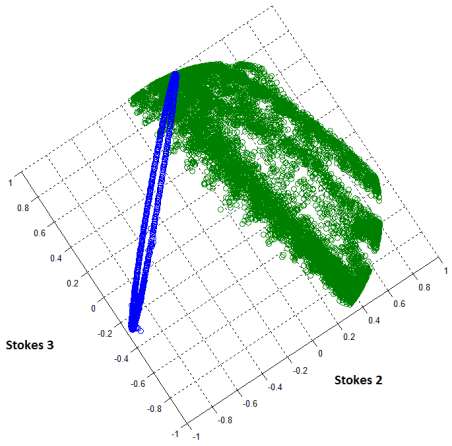

Figure 4.9: Output data for the reference sample. Data collected directly after the sample is plotted in blue, and data collected from the second fiber in green. The two seemingly have nothing in common.

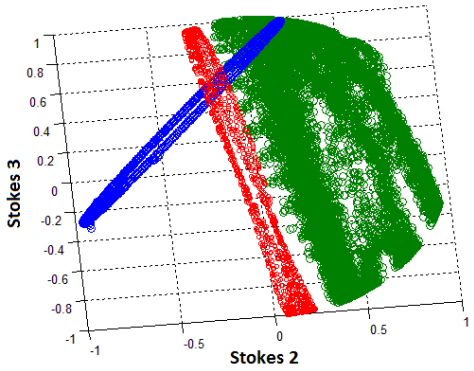

Figure 4.10: Output data for the reference sample. Data collected directly after the sample is plotted in blue, and data collected from the second fiber in green. The characteristic circle of the second fiber has been added in red. Because this fiber is not angle-polished, it is not very well-defined. Note that, as expected, the edges of the data from the second band run parallel to the second fiber's characteristic circle.

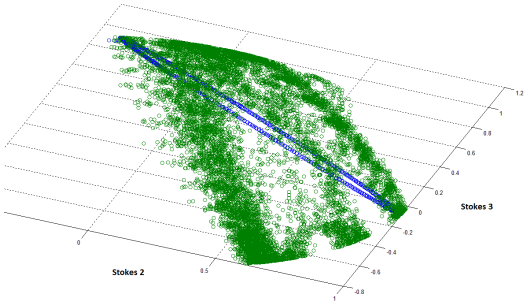

Figure 4.11: The output data for the reference wafer from the directly after the sample and from the second fiber, rotated so that they share the same frame of reference. The circle position matches the band width and position!

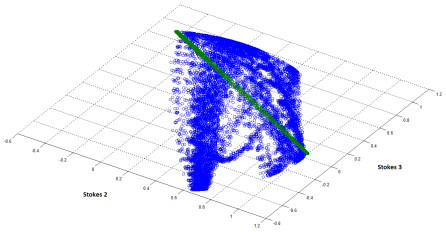

Figure 4.12: The same data, also rotated to the same frame of reference, for the twice-exposed silicon wafer. Again, the sample circle matches the output band!

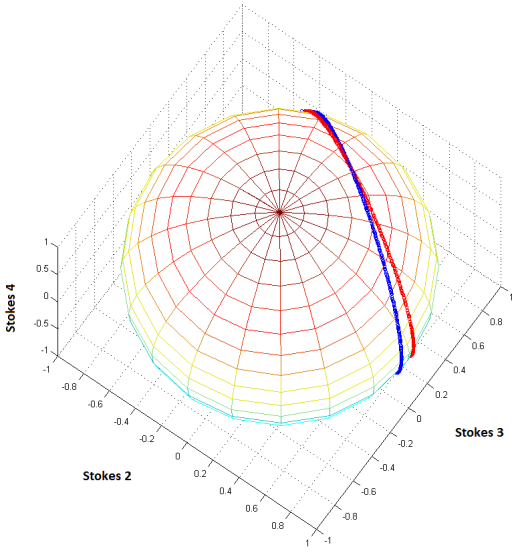

Figure 4.13: The different sample circles. Reference wafer is shown in blue, twice-exposed wafer is shown in red. The angle between the two is very small, approximately 6.9 degrees, which fits the characterisation done in the Woollam.

4.8 Uncertainty

Liu has shown that the half-fiber ellipsometer has an accuracy comparable to that of a commercial ellipsometer [13]. In the full-fiber system, no uncertainty is added for determining Ψ, as it can be determined in the same way as with the half-fiber one. For Δ, the crucial point lies in determining the width of the band width. As explained in Section 3, this is done in two steps: first, the characteristic circle of the second fiber has to be determined. This can be done very accurately by inputting a known polarisation state into the fiber and 3D-fitting the resulting circle with a plane. After this, the edges of the band have to be determined. This is more tricky, as it is easy to underestimate the width; after all, it is not possible to average the points on the edge of the band, as points over the edge will obviously not be mapped. However, since the direction of the edge is known, only one parameter[15] has to be optimised to fit the edge accurately. Given enough datapoints, it seems reasonable that we can estimate the band width to within 0.04 (a.u.), or two percent of the maximum width. The uncertainty in Δ caused by this fit error χ is equal to $\sin(\Delta + \chi) - \sin(\Delta)$. The uncertainty in the edge of the band can also be reduced by angle-polishing the fiber.

From the mathematics in Sec. 3, it can be seen that any uncertainty in the misalignment angles of the second fiber will show as uncertainty for Δ, as – for a misaligned fiber – they share the same axis of rotation. Thus, it is crucial to determine these angles very carefully. Provided this characterisation can be done to within one-tenth of a degree, and when doing measurements at multiple angles of incidence, we believe it is possible to use this setup to perform ellipsometric data with an accuracy comparable to that of commercial ellipsometers. This is because, when limiting this misalignment effect, no other inherent noise is added; all data from the sample circle is conserved.

[15] The position parameter 'd' of a 3D plane.

5 Conclusion

5.1 Summary

The goal of this work was to create a full-fiber ellipsometer with accuracy comparable to conventional ellipsometry. In this project, we have first investigated characteristics of polarisation-maintaining fibers, specifically of two successive fibers, using a simple model based on earlier work done by this group. This model, while based on only a few fundamental assumptions, was very suitable for predicting fiber behaviour. By studying simulation results, we gained an intuitive understanding of the mechanics behind such a two-fiber system, namely, that the output states from this system will form a characteristic band on the Poincaré sphere. The direction of this band is determined by the absolute misalignment of the second fiber, and the width is determined by the relative misalignment of the second fiber with the first. This understanding allowed us to examine the effects of a sample, specifically its ellipsometric parameters Ψ and Δ, on this band mathematically. It was concluded that Ψ could be obtained in two ways: one, by measuring the intensity of the light, and two, by examining the centre position of the band, as Ψ will shift the centre axis along the second Stokes vector. Delta proved more difficult, as it would not be conserved in a well-aligned full-fiber system. However, it was shown, that, provided the second fiber is misaligned with respect to the first one, it is possible to measure the changes in Δ as a function of the width of the band on the sphere. This is possible because this misalignment projects the values of the third Stokes vector onto the second one.

Following these mathematical investigations, experiments were done to confirm the suspected fiber behaviour, and to check whether modifying fiber misalignment would indeed result in a different projection of the third Stokes vector onto the second, and thus in a different band width. After this was successfully shown, an attempt was made to characterise three different silicon wafers with varying amounts of oxidation using our system. Unfortunately, this proved to be one bridge too far, as it was not possible to determine differences in Ψ and Δ between the samples in our poorly-characterised setup. Therefore, we settled for a proof-of-concept demonstration, where we accurately determined the setup misalignment, and used the method outlined above to link the circle of polarisation states measured after the sample to the band obtained after the second fiber. This matching was done accurately and for different samples, proving that our system can be used to perform ellipsometry measurements.

Lastly, experiments were done on a photonic crystal polarisation-maintaining fiber, to see if it could be used as a stable fiber for transporting the polarisation states from the sample to the polarimeter without having to compensate for constantly changing fiber effects. It could not.

To conclude, we are confident that using the techniques outlined in this thesis, it is possible to perform ellipsometry measurements, with an accuracy comparable to that of conventional ellipsometry, using a full-fiber system.

5.2 Future work

Although we have succeeded in demonstrating a proof-of-concept, we have not yet succeeded in accurately characterising a sample using the full-fiber ellipsometer. In order to do this, it is highly desirable to rebuild the setup to work with a angle of incidence closer to grazing incidence, and absolutely crucial to determine fiber misalignment to within at least one-tenth a degree for the facets of the second fiber. It will also be required to angle-polish the second fiber. If this can be done, it should be possible to accurately characterise a sample. Provided this is successful, work can then begin on implementing the fiber ellipsometer into, ideally, an *in situ* measurement setup. Alternatively, work can be done to extend the current setup for work at different wavelengths and/or different angles of incidence. Finally, it might be worthwhile to investigate the polarisation properties of optical switches, to fully complete the ideal of a time-shared, non-line-of-sight ellipsometer that can be used on multiple setups virtually simultaneously.

References

[1] K. Chopra and S. Das, *Thin Film Solar Cells*. New York City: Springer, 1983.

[2] S. L. Tao and T. A. Desai, "Microfabricated drug delivery systems: from particles to pores," *Advanced Drug Delivery Reviews*, vol. 55, no. 3, pp. 315 – 328, 2003. ¡ce:title¿Biomedical Micro- and Nano-technology¡/ce:title¿.

[3] I. Lynch, P. de Gregorio, and K. A. Dawson, "Simultaneous release of hydrophobic and cationic solutes from thin-film plum-pudding gels: a multifunctional platform for surface drug delivery?," *The Journal of Physical Chemistry B*, vol. 109, no. 13, pp. 6257–6261, 2005. PMID: 16851694.

[4] C. Montcalm, S. Bajt, P. B. Mirkarimi, E. Spiller, F. J. Weber, and J. A. Folta, "Multilayer reflective coatings for extreme-ultraviolet lithography," in *Proc. spie*, vol. 3331, pp. 42–51, 1998.

[5] J.-Q. Xi, M. F. Schubert, J. K. Kim, E. F. Schubert, M. Chen, S.-Y. Lin, W. Liu, and J. A. Smart, "Optical thin-film materials with low refractive index for broadband elimination of fresnel reflection," *Nature Photonics*, vol. 1, no. 3, pp. 176–179, 2007.

[6] I. Schnitzer, E. Yablonovitch, C. Caneau, T. Gmitter, and A. Scherer, "30% external quantum efficiency from surface textured, thin-film light-emitting diodes," *Applied Physics Letters*, vol. 63, no. 16, pp. 2174–2176, 1993.

[7] T. Tsarfati, R. Van De Kruijs, E. Zoethout, E. Louis, and F. Bijkerk, "Reflective multilayer optics for 6.7 nm wavelength radiation sources and next generation lithography," *Thin Solid Films*, vol. 518, no. 5, pp. 1365–1368, 2009.

[8] Gaertner Scientific, "In situ stokes ellipsometer l104st." http://www.gaertnerscientific.com/ellipsometers/l104st.htm, june 2007.

[9] T. Yoshino and K. Kurosawa, "All-fiber ellipsometry," *Appl. Opt.*, vol. 23, pp. 1100–1102, 1984.

[10] E. Kim, D. Dave, and T. E. Milner, "Fiber-optic spectral polarimeter using a broadband swept laser source," *Optics Communications*, vol. 249, no. 13, pp. 351 – 356, 2005.

[11] N. Gisin, G. Ribordy, W. Tittel, and H. Zbinden, "Quantum cryptography," *Rev. Mod. Phys*, vol. 74, pp. 145–195, 2002.

[12] J. Zhang, S. Guo, W. Jung, J. Nelson, and Z. Chen, "Determination of birefringence and absolute optic axis orientation using polarization-sensitive optical coherence tomography with pm fibers," *Opt. Express*, vol. 11, pp. 3262–3270, Dec 2003.

[13] F. Liu, C. J. Lee, J. Chen, E. Louis, P. J. M. van der Slot, K. J. Boller, and F. Bijkerk, "Ellipsometry with randomly varying polarization states," *Opt. Express*, vol. 20, pp. 870–878, Jan 2012.

[14] B. Robson, *The Theory of Polarization Phenomena*. Oxford: Clarendon Press, 1974.

[15] W. Shurcliff, *Polarized light: production and use*. Cambridge, Massachusetts: Harvard University Press, 1962.

[16] H. Tompkins and E. Irene, eds., *Handbook of Ellipsometry*. Norwich, NY: William Andrews Publications, 2005.

[17] F. Liu, "Theoretical and experimental investigation of fiber based ellipsometry for characterization of carbon layer thickness," Master's thesis, University of Twente, 2011.

[18] T. Martynkien, M. Szpulak, and W. Urbanczyk, "Modeling and measurement of temperature sensitivity in birefringent photonic crystal holey fibers," *Appl. Opt.*, vol. 44, pp. 7780–7788, Dec 2005.

[19] H. Arwin and D. Aspnes, "Unambiguous determination of thickness and dielectric function of thin films by spectroscopic ellipsometry," *Thin Solid Films*, vol. 113, p. 101, 1984.

A Appendix1: Photonic Crystal Fibers

We also chose to investigate stability of a different type of polarisation maintaining fiber in the hopes of finding one that could be considered stable over the course of a single ellipsometric measurement. As shown in the other sections, conventional PM fibers are far too unstable to attempt this. However, there is another type of PM fiber, known as a photonic crystal polarisation-maintaining fiber, which might fare better. These PC-PM fibers are capable of achieving birefringence values up to an order of magnitude higher than conventional polarisation-maintaining fibers [18]. This is because rather than depending on refractive index differences caused by stress differences, PC-PM can rely on confining the light because of their crystal structure. They can thus also have a hollow core, causing birefringence values to be much less stress- and temperature-dependant.

Since only single-fiber stability was measured, this could be done in a relatively simple setup, which can be seen in Fig. A.1. In short, it consists of a light source (HeNe laser, wavelength: 632.8 nm, output power: 5 mW), a Wollaston prism that sets the initial polarisation to linearly polarized light with a purity of 100000:1, and a quarter-wave plate to adjust the input polarisation state of the light. After polarisation control, the light is coupled into the fiber we want to investigate. Experimental details were identical to those described in Section 4: polarisation measurements were done using the Thorlabs PAX5710VIS-T polarimeter, which operates in the $400 - 700$ nm wavelength range. It has a maximum sample collection speed of 330 samples/second, and the maximum number of data points that can be collected in one measurement series is 1024. Circularly polarised light with a power of 2.0 ± 0.410^{-6} Watt was input into the fibers. The crucial difference with the experiments in the previous chapters was that here – since we expressly want to investigate fiber stability rather than the behaviour of modified fibers – the fiber was not actively modified in any way. However, it is important to note no extra measurements were taken to secure the fiber during testing, meaning, that, since they were both suspended over and lying on the optical table, both airflow as well as vibrations could have modified the fiber. We take this to be representative of actual conditions in which a fiber ellipsometer would be used.

Care must be taken when attempting to quantify fiber stability, as characteristics such as temperature dependence or fiber birefringence do not give enough information about whether the fiber can be considered stable over the course of one measurement. What we require is for the fiber to have a constant effect on ellipticity during the time of our measurement; ie, a

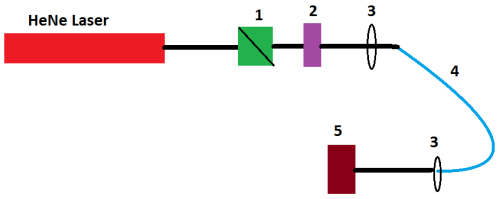

Figure A.1: A schematic representation of the measurement setup used for fiber testing. Optical components consist of (1) a Wollaston prism, (2) a quarter-wave plate, (3) coupling lenses, (4) A Polarisation-Maintaining fiber (either PM or PC-PM), (5) a Thorlabs polarimeter.

transformation that is constant in this timeframe. Assuming a typical measurement (including the time it would take to modify the first fiber) takes 5 seconds, the fiber would need to be stable in this timeframe. As a first test, fiber stability over several hours was measured. As the polarimeters slowest measurement speed was 33 samples per second, and it did not contain enough memory to continue this measurement for multiple hours[16], it was set to heavily average all measurements using options present in the polarimeter software. More accurately: both the direct signal from the photo diode as well as the resulting Fourier transforms were averaged over thirty measurements. This artificially increased measurement time to nearly eight hours. Results of these measurement can be seen in Fig. A.2 and **??** for the PC-PM and PM fiber, respectively. Only the values for ellipticity (Ψ) are displayed; in this case, it is easier to compare single values rather than comparing all three Stokes vectors. Results for the Δ values were similar to those shown here.

After an initial stabilisation period, possibly related to a temperature decrease in the laboratory as it was shutting down for the night, the ellipticity does indeed remain more or less constant over several hours. However, the results for the PC-PM fiber also show a clear short-time variance, which is more relevant for our measurements than long-term stability: a 4 to 5 degree spread in ellipticity can be observed throughout the series. One possible explanation for this might be fiber vibration due to airflow in the lab, as the fiber was suspended over the measurement table. The fact that, unlike the conventional PM fiber, the photonic crystal fiber was not armoured, substantially reducing the weight, might contribute to this. Still, no matter

[16]The Thorlabs Polarimeter has a maximum of 1024 points per measurement series.

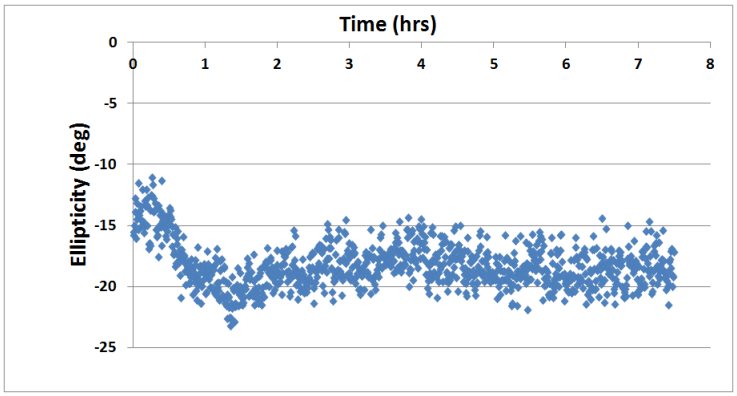

Figure A.2: Long term output stability for the Photonic Crystal Fiber. Values for ellipticity given as time (in hours) progresses. Even though the 'baseline' of the signal is quite constant, it is quite broad - at some points, more than 5 degrees. This possibly indicates a large short-timeframe variance.

the cause, this would indicate that slight changes in stress still affect fiber stability, as it seems unlikely that the fiber was vibrating heavily. In any case, this situation warranted further studying, and a second measurement specifically targeting short-term stability was performed.

Fig.A.3 shows two data series taken from a measurement set. Polarisation states were measured at 330 samples per second for a little over 3 seconds. Note again that the fibers were not modified during this measurement. The figures clearly show the same short-time variance also present in Fig. A.2; for example, a change of approximately 8 degrees can be be seen in (a). It is important to note that the variances in (a) and (b) are clearly different; this means that in this timeframe, the fiber's effect on polarisation is not a predicable or systematic effect, but seems truly random. This is demonstrated in (c) and (d), where the derivatives of the data in (a) and (b) are shown. Again, this derivative is not constant, indicating that while the fiber could possibly show periodic effects over a longer timeframe[17], in this timeframe – which is close to the time an actual measurement would take – the change is unpredictable. This means that it is difficult, if not impossible, to compensate for these effects during a continuous ellipsometric measurement.

Why the PC-PM fiber shows short-term instability is not quite clear.

[17] As is the case with the regular PM fiber

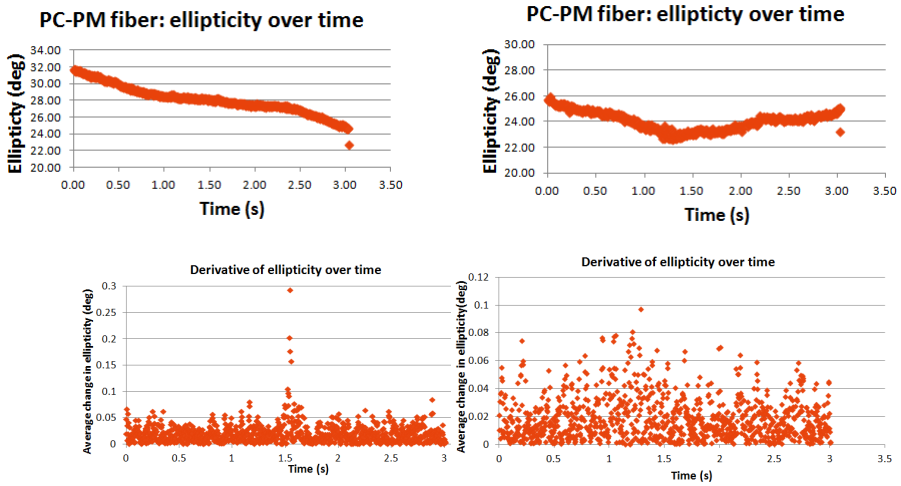

Figure A.3: Figures (a) and (b) show ellipticity values for a measurement performed on a photonic crystal polarisation-maintaining fiber. Note that the two graphs have different scales. Sample speed was 330 samples per second for a little over three seconds; input light was circularly polarised. Both (a) and (b) show relatively large (4 - 8 degrees) short-term variance. (c) and (d) show the derivative for (a) and (b), respectively. Note the different ranges for the y-axis. It is clear the derivative is not constant during the time of this measurement.

It is possible that the fiber was moving slightly during the experiment; as explained above, the fact that it is not armoured results in a much lower weight thus possibly causing stress effects. This could be caused either by airflow in the lab or residual oscillation from aligning and setting up the system. Furthermore, although it seems unlikely that temperature variations in the climate-controlled lab occur rapidly enough to affect the fiber characteristics within a few microseconds, it cannot be ruled out, even with the reduced temperature susceptibility of the PC-PM fiber. Liu estimated the temperature variation necessary to obtain a full circle in a conventional PM fiber, meaning the ellipticity changes by 180 deg, to be about 2∘. According to the PC-PM spec sheet, these fibers have 'a temperature coefficient of birefringence (...) up to 30 times less than that of other leading stress-birefringent fibers,' indicating that the eight-degree difference in ellipticity values seen in our experiments would correspond to a temperature shift of approximately two degrees in five seconds. Though this seems high, it is not entirely unreasonable in our poorly-controlled lab conditions.

In summary, even though photonic-crystal polarisation-maintaining fibers might be much more stable that conventional PM fibers, they are – in our lab environment, in any case – far from stable enough to be considered constant over the course of one measurement. Thus, they are not suitable for use in the fiber ellipsometer.

B Appendix 2

```
function [output_matrix] = simplefibersim(zz)
%Function: simulate the first PM-fiber
%Declaring the function, importing the input polarisation state (1 x 4 vector)

input_polarisation = zz;  %Switching to working variable

output_matrix = zeros(4,1600);  %Setting up the output matrix

mis_angle = (1/4) * pi;   %Setting misalignment angle

beat_length = 1.8;  %In mm for convenience
beat_length_step =0.00011;     %Approx. 1% increase in beat length
%at the end of the cycle
%when we use 1600 steps; ie, this is approx.
%beat_length*0.01/1600$

length_of_fiber = 2000;  %In mm for convenience

front_matrix = [1 0 0 0  ; 0 cos(2*mis_angle) sin(2*mis_angle) 0 ;
0 -sin(2*mis_angle) cos(2*mis_angle) 0; 0 0 0 1];
%Setting matrices for misalignment angle
back_matrix = [1 0 0 0  ; 0 cos(2*mis_angle) sin(2*mis_angle) 0 ;
0 -sin(2*mis_angle) cos(2*mis_angle) 0; 0 0 0 1];

i = 1;
for i=1:1600;
beat_length = beat_length + (i*beat_length_step);
%Calculating beat length for each step
delta = 2*pi*(length_of_fiber/beat_length);
delta_matrix = [1 0 0 0; 0 1 0 0 ; 0 0 cos(delta) sin(delta);
0 0 -(sin(delta)) cos(delta)];
%Setting the matrix for fiber, dependant on beat length

output_matrix(:,i)=front_matrix*delta_matrix*back_matrix*input_polarisation(:,1);
%Calculating output state
end

end   %End of this part of the simulation
```

```
function [output_matrix_normalised] = sample(x,p,d)
%Function: simulate a sample
%Input: collection of input states, psi and delta of the sample

psi = p; %Importing to a working variable
delta = d; %Likewise

light_polarisation = x; %Inporting the light polarisation states
%switch to a working variable rather than global

output_matrix = zeros(4,1600); % Setting up the output matrix

sample_matrix = [1 -cosd(2*psi) 0 0 ; -cosd(2*psi) 1 0 0 ;
0 0 sind(2*psi)*cosd(delta) sind(2*psi)*sind(delta);
0 0 -sind(2*psi)*sind(delta) sind(2*psi)*cosd(delta)];
 %setting the sample matrix with user-defined psi and delta

i=1;
for i=1:1600;
output_matrix(:,i) = sample_matrix * light_polarisation(:,i);
end

%rescale everything so that the Stokes parameters can be plotted on a sphere:
%find factor to rescale by
j=1;
for j=1:number_of_input_states
rescale_factor(j)=output_matrix(2,j)^2+output_matrix(3,j)^2+output_matrix(4,j)^2;
%Since the 2nd, 3rd and 4th stokes vecors squared and added need to equal one,
%they are squared and summed. Rescale factor is then the sqrt(1)/(this sum)
output_matrix_normalised(:,j) = (1/sqrt(rescale_factor(j))) * output_matrix(:,j);
end

end %End of this part of the simulation
```

```
function [output_matrix] = second_simplefibersim(x)
%Function: simulate the second PM-fiber

input_polarisation = x;   %Importing the light polarisation states

output_matrix = zeros(4,1600); %Setting up the output matrix

mis_angle = (1/8) * pi;  %Setting misalignment angle

beat_length = 1.8; %In mm for convenience
beat_length_step =0.0001101; %Approx. 1.1% increase in beat length
%at the end of the cycle when we use 1600 steps; ie,
%this is beat_length* 0.011/1600$

length = 2000; %In mm for convenience

front_matrix = [1 0 0 0  ; 0 cos(2*mis_angle) sin(2*mis_angle) 0 ;
0 -sin(2*mis_angle) cos(2*mis_angle) 0; 0 0 0 1];
%Setting matrices for fiber misalignment angle
back_matrix = [1 0 0 0  ; 0 cos(2*mis_angle) sin(2*mis_angle) 0 ;
0 -sin(2*mis_angle) cos(2*mis_angle) 0; 0 0 0 1];

i = 1;
for i=1:1600;
beat_length = beat_length + (i*beat_length_step);
delta = 2*pi*(length/beat_length);
delta_matrix = [1 0 0 0; 0 1 0 0 ; 0 0 cos(delta) sin(delta);
 0 0 -(sin(delta)) cos(delta)];
output_matrix(:,i)=front_matrix*delta_matrix*back_matrix*input_polarisation(:,i);
% multiplying relevant parts of the input polarisation vector
%and the fiber Mueller matrix

end

end
```